J. Plasma Physics (1997), *vol.* 57, *part* 4, *pp.* 765–784. Printed in the United Kingdom
© 1997 Cambridge University Press

Variational principle for crossed-field devices

D. J. KAUP[1] and GARY E. THOMAS[2]

[1]Institute for Nonlinear Studies and Departments of Physics and Mathematics, Clarkson University, Potsdam, NY 13699-5815, USA

[2]Communications & Power Industries, 150 Sohier Road Beverly, Massachusetts 01915, USA

(Received 15 December 1995)

We present a Rayleigh–Ritz variational model of the electron sheath in crossed-field devices. Using laminar layer orbits, this model predicts equilibria in agreement with the classical Brillouin model. Other predictions include the existence of existence of non-classical, stable equilibria as well as limit cycles. This variational model also predicts the existence of a stable propagating diocotron mode, which is absent from the Brillouin model but is present in the double-box model of Kaup and Thomas. Comparisons of these results with those of the cold-fluid theory are discussed.

1. Introduction

The design and manufacturing of crossed-field devices remains an experimental domain in spite of the tremendous amount of theoretical work done in this area: see, for example, Buneman *et al.* (1966), Loveland and Ott (1974), Swegle and Ott (1981), Swegle (1983), Cherrin and Lau (1984), Antonsen *et al.* (1985), Davidson (1985*a*, *b*), Davidson and Tang (1985), Riyopoulos (1991, 1993*a*, *b*), Riyopoulos *et al.* (1992), Uhm (1992), Lau and Chernin (1992), Lau *et al.* (1993) and Christenson and Lau (1994). As a result, one concludes that the exact physical mechanism by which these devices operate is probably still unclear, even in the present day. Numerical simulations of these devices can now be readily obtained, and frequently do provide useful information (Palevski *et al.* 1981; Dombrowski 1988). However, they have yet to provide means for determining operating ranges for current or future devices. Thus the design of crossed-field devices still remains an experimental domain.

Even the simple problem of the start-up of a crossed-field amplifier (CFA) or a magnetron is poorly understood. The classical theory of such devices (Buneman *et al.* 1966) is based on a linear instability that, at best, for the operating mode, lies deep inside the electron sheath and well away from the parameter regime used by the design engineers. The predicted instability is indeed there (Jablonski 1992); however, it seems to have nothing to do with the start-up of a CFA or magnetron. The dominant effect of the instability appears to be to simply diffuse the edge of the sheath, with no growth of the desired mode.

Analytical studies have provided useful information. Perturbation theory of a Vlasov model (Kaup and Thomas 1992*a*) has provided insight into the stability properties of the sheath. A double-box model (Kaup and Thomas 1992*b*) of the sheath predicts the existence of a propagating diocotron mode and has provided an understanding of how the operation of a crossed-field device could initialize. According to the latter, by some means, a convective cell (Davidson and Krall 1970;

https://doi.org/10.1017/S0022377897005503 Published online by Cambridge University Press

Bogema and Davidson 1970; Kaup 1990) is formed. Once a convective cell has formed, there is a high-density inner sheath and the outer adjacent lower-density region of the convective cell (Thomas *et al.* 1985). The modulational stability of a radio frequency (RF) wave in such a density profile has been studied (Kaup and Thomas 1989, 1992*b*). What was found was that the RF wave is strongly modulationally unstable. Typical estimates reveal that the nonlinearity is sufficiently strong to create roughly one soliton per wavelength. Of course, in this case, one no longer has a slowly varying envelope – a key simplifying assumption of the theory. However, there is still certainly some truth in this calculation since in numerical simulations, one sees a density of 'spokes' on this order. This suggests that the initial formation of the spokes may well be due to a modulational instability, but with the system rapidly becoming strongly nonlinear as a spoke grows. Nevertheless, these ideas did lead to a predicted voltage operating range in much better agreement with experiment than any other theory or even numerical simulations.

In light of this, it would seem appropriate to try another analytical approach that could be appropriate for strongly nonlinear systems. Such a method is the Rayleigh–Ritz variational principle with suitable chosen trial functions. Of course, the latter are the key to the success or failure of the method. The results will only be as good as the trial functions are close to the actual solutions. What we shall do is to devise a Rayleigh–Ritz variational principle for the cold-fluid equations in a crossed-field device. We find that a rather simple choice of trial functions, based on a laminar flow, provides some quite interesting results.

First, the model very closely approximates the classical Brillouin theory and also contains the classical Brillouin density background solution. However, there are other possible, non-classical, background solutions, contained in this model that, as far as we know, have never been explored. Among these are some that are in regions of parameter space which could be occasionally accessible to operating devices. The interest in these regions is that if a device ever ended up in one of these regions, it might not operate as expected or possibly not operate at all. Indeed, these regions provide a possible explanation for a 'missing pulse phenomenon' occasionally seen in the laboratory. Even though the direct-current (DC) voltage, DC magnetic field, and driver signal are all present, sometimes a CFA does not start, i.e. it misses a pulse. However, the CFA successfully amplifies the very next driver pulse. Any attempt to explain this based on a deficiency of electrons during the interpulse period has a major difficulty. How could there be enough electrons to start the tube after a pulse is missed when there weren't a sufficient number of electrons to start during the missed pulse? On the other hand, the explanation may be that the electrons actually were there, but they were briefly in momentum states that prevented amplification. We shall give examples later on of how such states could occur and describe how they would prevent amplification.

In addition to the background characteristics of this model, we also consider linearized RF modes. Here we find that the linearized RF dispersion curves have two main branches: an acoustic-like or diocotron branch and a cyclotron branch. The surprising thing is the existence of the almost dispersion-free diocotron branch. This mode does not exist in the standard Brillouin cold-fluid theory (Buneman *et al.* 1966) as a free mode. However, it appears here as one of two major modes. Furthermore, one should note that it is the assumed existence of such a mode that is a key assumption in the design of a CFA. An important question becomes why

https://doi.org/10.1017/S0022377897005503 Published online by Cambridge University Press

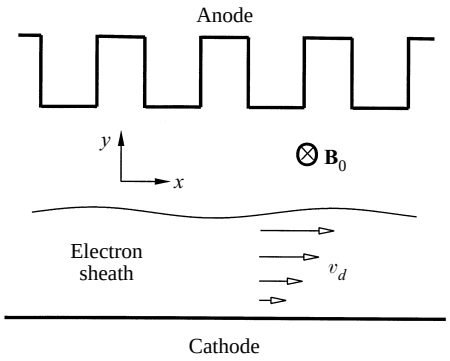


Figure 1. The geometry and configuration of a planar magnetron or CFA. The magnetic field is directed into the paper and the electron drift velocity is to the right. The z axis is perpendicular to the paper, the x axis is parallel to the cathode surface, and the y axis is perpendicular to the cathode.

does it appear here and why does it not appear as a free mode in the Brillouin cold-fluid theory. This question will be addressed in the appropriate sections.

In the next section, we shall detail the trial functions to be used and obtain the averaged Lagrangian. Then, in Sec. 3, we shall discuss the background solution obtained from the Raleigh–Ritz variational method, and, in Sec. 4, the linearized RF solution. Concluding remarks will be made in Sec. 5.

2. Trial functions for a laminar flow

Consider a planar configuration where the cathode is located at $y = 0$, and the anode at $y = l$, both parallel to the (x, z) plane (see Fig. 1). We shall model the cathode as a perfectly conducting medium with a zero work function. Thus electrons will move out of and into the cathode upon the demands of the electric field at the surface of the cathode, and with no loss or gain of energy. Let the magnetic field be in the negative z direction, $\mathbf{B} = -B_0\hat{\mathbf{z}}$. Let there be a positive voltage V applied to the anode, with the cathode at ground potential, with an electron sheath being formed above the cathode. We shall only consider particle motion in the (x, y) plane, where there is no dependence on the z coordinate. Also, we shall use the electrostatic approximation, ignoring any RF magnetic field. Under these conditions, the total Lagrangian is simply

$$L = \sum_j [\tfrac{1}{2}mv_j^2 - m\Omega y_j v_{xj} + e\phi(x_j, y_j)] + \frac{1}{8\pi}\int dx \int dy\, [(\partial_x\phi)^2 + (\partial_y\phi)^2], \tag{1}$$

where ϕ is the electrostatic potential, $\Omega = eB_0(mc)$ is the electron cyclotron frequency, $m\,(e)$ is the electronic mass (absolute electronic charge), (x_j, y_j) are the spatial coordinates of the jth electron and (v_{xj}, v_{yj}) are its velocity components. Varying the electron's position in (1) gives the momentum equations, and varying $\phi(\mathbf{x})$ gives Poisson's equation.

Now we shall choose trial functions for the electron orbits and the electrostatic potential. We take the electron orbits to be in laminar layers. Inside each layer,

https://doi.org/10.1017/S0022377897005503 Published online by Cambridge University Press

the electrons move independently of the electrons in the other layers (except for interactions through the electrostatic potential) and oscillate about a guiding centre. Let the electrons' positions be specified by

$$x_j = \xi_{xj} + a_0 + a_1\xi_{yj} + e_1 y_j \sin\theta_x, \tag{2a}$$

$$y_j = \rho(\xi_{yj} - b_c) - f_1 y_j \cos\theta_y, \tag{2b}$$

where (ξ_{xj}, ξ_{yj}) is the initial position of the jth electron, and a_0, a_1, b_c, ρ, e_1 and f_1 are arbitrary functions of time. The phases are

$$\theta_x = kx_j - \omega t + \mu, \tag{3a}$$

$$\theta_y = kx_j - \omega t + \nu, \tag{3b}$$

where $k(\omega)$ is the wave vector (frequency) of an RF wave and μ and ν are possible time-dependent phase shifts. A discussion of (2) is now in order.

The first term in (2a) represents the initial x position of the electron. The second term, $a_0(t)$, allows all electrons, regardless of their y positions, to be uniformly displaced in the x direction. The third term, $\xi_{yj}a_1(t)$, allows a shear flow to be present, where the x component of the velocity of the electrons will be proportional to $da_1(t)/dt$ and ξ_{yj}. Thus electrons with larger values of ξ_{yj} will move faster. The last term, $e_1 y_j \cos\theta_x$ allows the x position to oscillate, with an amplitude proportional to the current y position.

In (2b), the term $\rho(t)$ allows the vertical density of the laminar orbits to change. As $\rho(t)$ increases, layers move apart, while if $\rho(t)$ decreases, they move closer together, giving a higher density. Initially, we take $\rho(0) = 1$ and $b_c(0) = 0$, so that ξ_{yj} can be interpreted as the initial y position. The factor $b_c(t)$ allows all layers to move uniformly up or down. It is this term that models the emission and absorption of electrons at the perfectly conducting, zero-work-function, cathode surface. The last term, $f_1 y_j \cos\theta_y$, allows the electron layers to respond vertically to an RF field.

As we have mentioned above, the term $b_c(t)$ allows electrons to enter and exit from the vacuum region between the cathode and the anode, depending on the sign of the electric field at the cathode. As we shall see later, $b_c(t)$ will be driven by the electric field at the cathode, and, as expected, its evolution will be such as to fill the vacuum region with electrons, or remove electrons from the vacuum region, so as to drive the electric field at the cathode back to zero.

The mathematics of the model work in the following simple manner. For any layer where $\xi_{yj} < b_c(t)$, these electron layers are inside the cathode (which is at $y = 0$) and will be excluded from the sum in (1). But if at some time later $b_c(t)$ becomes less than ξ_{yj} then that layer will have been 'emitted' from the cathode and will have entered the physical region. Then this layer will be counted in (1). (As we shall see later, this will only occur if the electric field at the cathode is such that the electrons would have ordinarily been drawn out. This also occurs with no loss of energy, so the work function of the surface is zero.)

We model the electrostatic potential as follows. Inside the sheath, we take

$$\phi_l(x, y) = C_1 y + C_2 y^2, \tag{4a}$$

and outside the sheath, we take

$$\phi_u(x, y) = V_0(1 + V_1 \cos\theta) - d_1(l - y), \tag{4b}$$

https://doi.org/10.1017/S0022377897005503 Published online by Cambridge University Press

where

$$\theta = kx - \omega t, \tag{5}$$

and the coefficients C_1, C_2, V_0, V_1 and d_1 may be time-dependent as well as functions of θ. In (4*a*), the C_1 allows an electric field to be present at the cathode, which then could drive the term $b_c(t)$ above. The term C_2 gives a non-zero value to $\nabla^2\phi$, required by Poisson's equation. In (4*b*), V_0 is the DC potential while V_1 is the *relative* RF potential at the anode. The term $d_1(l-y)$ vanishes at the anode, and represents the uniform DC electric field present above the sheath.

The position of the upper layer of the sheath will be determined by the maximum value of $\xi_{yj} = \xi_b$, whose corresponding maximum y position will be, from (2*b*),

$$b = \rho(\xi_b - b_c), \tag{6}$$

which is the thickness of the sheath.

At the upper layer of the sheath, we need to ensure continuity of ϕ and $\partial_y\phi$ as given by (4*a*, *b*). This will give two conditions, which will determine two of the coefficients in (4) in terms of the other two. We shall find it most convenient to use these conditions to express C_2 and d_1 as functions of C_1, V_0 and V_1.

The last thing to specify is how the sum over j in (1) is to be done. Each electron is labelled with its initial position (ξ_{xj}, ξ_{yj}) at $t = 0$. We take the initial distribution of electrons to be given by an initial density, $n(\xi_{xj}, \xi_{yj})$, then replace the sum by an integral over $d\xi_{xj}d\xi_{yj}$. Of course, the choice of $n(\xi_{xj}, \xi_{yj})$ is totally arbitrary. It simply describes how the electrons are initially distributed before releasing them. Then, once they are released, they each are constrained to evolve along the orbits given by (2).

We shall choose $n(\xi_{xj}, \xi_{yj})$ to be independent of ξ_{xj} and a box shape for the ξ_{yj} dependence. Thus we take

$$n(\xi_{xj}, \xi_{yj}) = \begin{cases} n_i & (\xi_{yj} < \xi_b), \\ 0 & (\xi_{yj} > \xi_b), \end{cases} \tag{7}$$

where n_i is the initial density in the sheath and ξ_b is the value of ξ_{yj} at the topmost layer of electrons. Note that the actual density of the sheath will be

$$n = n_i/\rho, \tag{8}$$

since the factor ρ describes how the orbits will condense or rarefy. Thus (1) becomes

$$\begin{aligned} L = &\int d\xi_x \int_{b_c}^{\xi_b} d\xi_{yj}\, n_i[\tfrac{1}{2}mv_j^2 - m\boldsymbol{\Omega} y_j v_{xj} + e\phi_j] \\ &+ \frac{1}{8\pi}\int dx \int_0^l dy\, [(\partial_x\phi)^2 + (\partial_y\phi)^2]. \end{aligned} \tag{9}$$

The final evaluation of (9) is described in Appendix A. In the next section, we discuss the result for (9) when the RF field is absent ($e_1 = 0 = f_1 = V_1$) and in Sec. 4, we treat the linearized version of the RF fields. We also scale all parameters, letting our unit of length be l (the cathode–anode spacing), the unit of time $\boldsymbol{\Omega}^{-1}$ and the unit of density $m\boldsymbol{\Omega}^2/4\pi e^2$, the unit of voltage $l^2\boldsymbol{\Omega}^2 m/e$, and we scale the Lagrangian by $12/(m\boldsymbol{\Omega}^2 l^3 L_x)$, where L_x is the length of the x integration. Thus, in these units, the classical Brillouin density is when $n = 1$ and the Hull voltage is where $V_0 = \frac{1}{2}$.

https://doi.org/10.1017/S0022377897005503 Published online by Cambridge University Press

3. The background solution

An important test of any choice of orbital trial functions for the Rayleigh–Ritz variational method will be how well they can represent the evolution of the background solution. If we freeze out the RF modes ($e_1 = 0 = f_1 = V_1$) then we have a pure laminar flow, the background solution of which should be an average of the cold-fluid background solution. This is indeed the case. However, we find additional features that are not found or available in the equilibrium solutions of the cold-fluid equations. In the cold-fluid equations, the background density profile is always arbitrary. However, for stability (Davidson 1985*b*) it is known that the equilibrium density gradient must be zero or negative and that the density can never exceed the Brillouin limit (Brillouin 1945; Macfarlane and Hay 1950; Buneman 1955; Kaup and Thomas 1992*a*), which is where the electron plasma frequency equals the electron cyclotron frequency. But these facts come from higher-order studies (e.g. the linear perturbation of the cold-fluid equations) and not from the equations for the background solution. But, for our choice of trial functions, regardless of the initial configuration, providing only that all electrons were originally emitted from the cathode at zero velocity so that they have zero momentum, we find that all such configurations will evolve toward the Brillouin limit of $n = 1$, which is the only fixed point of these equations. One can trace the source of this result to the variation of b_c, which allows electrons to be emitted or absorbed by the cathode, a feature that cannot be easily incorporated into the cold-fluid equations.

There are also other interesting solutions. Let us suppose that after a pulse is amplified in a CFA, there was some residual distribution of electrons remaining in the device. Then, as the next pulse is injected to be amplified, one would not necessarily have the same above initial configuration. Some of these configurations even have slightly lower energies than the classical Brillouin configuration, and they also have stable limit cycles, at least within the limits of this model. The implications of this is that if a device, upon start-up, did end up in one of these alternative configurations then it would certainly either operate with different characteristics or possibly not at all. However, further study will be necessary before one can determine that these alternative configurations do occur in and are significant for actual devices.

Let us now detail the above points. Letting $e_1 = 0 = f_1 = V_1$, in (8), we obtain

$$\begin{aligned} L = {} & \frac{2}{l_b^2}[b(1-\tfrac{3}{4}b)C_1^2 - 2bV_0C_1(1-\tfrac{3}{4}b) + 3V_0^2(1-\tfrac{2}{3}b)] \\ & + n_i\frac{2b^2}{\rho l_b}[V_0 + 2C_1(1-\tfrac{3}{4}b)] + n_i\left[\frac{6b}{\rho}\left(\dot{b} - \frac{1}{2}\dot{\rho}\frac{b}{\rho}\right)^2 + \frac{1}{2}b^3\frac{\dot{b}^2}{\rho^3}\right] \\ & + n_i\left(2\dot{a}_1^2\frac{b^3}{\rho^3} - 6\frac{b^2}{\rho^2}\dot{a}_1\dot{a}_2 + 6\frac{b}{\rho}\dot{a}_2^2 + 2\frac{\dot{a}_1 b^3}{\rho^2} - 6\frac{b^2}{\rho}\dot{a}_2\right), \end{aligned} \tag{10}$$

where

$$l_b = 1 - \tfrac{1}{2}b, \tag{11}$$

$$a_2 = a_0 + \xi_b a_1. \tag{12}$$

In the above, from (2*a*), we see that $\dot{a}_2$ is simply the velocity at the top of the sheath and $\dot{a}_1/\rho$ is the averaged vorticity ($\partial_y v_x$). Since a_2 and a_1 are cyclic coordinates,

https://doi.org/10.1017/S0022377897005503 Published online by Cambridge University Press

their momenta are constants of the motion. These are

$$P_{a1} = n_i \left(4\frac{b^3}{\rho^3}\dot{a}_1 - 6\frac{b^2}{\rho^2}\dot{a}_2 + 2\frac{b^3}{\rho^2} \right), \tag{13a}$$

$$P_{a2} = n_i \left(12\frac{b}{\rho}\dot{a}_2 - 6\frac{b^2}{\rho^2}\dot{a}_1 - 6\frac{b^2}{\rho} \right). \tag{13b}$$

These conserved momenta are the variational analogies of the conservation of the linear x momentum of the cold-fluid equations. There, one normally takes this momentum to be zero, thereby constraining the x component of the velocity to be proportional to the electric field. However, there are configurations where this does not have to be true. Let us make two observations about (13). First, if initially there is no sheath then $b = 0$, causing both momenta to vanish. Secondly, in the case of an initial Brillouin flow, from (2a), we should take $\dot{a}_0 = 0$ and $\dot{a}_1 = \rho$, whence $\dot{a}_2 = \xi_b \rho$. Then each momenta becomes proportional to the factor $b - \xi_b \rho$ $(= b_c)$. Consequently, if no additional electrons entered or left through the cathode then $b_c = 0$ (which is the initial value), and these two momenta also vanish for an initial Brillouin flow. So we see that for the two standard initial configurations, these momenta vanish. Thus if these two momenta take on non-zero values then they will represent configurations different from both Brillouin flow and from an initially empty sheath.

Let us continue. Since C_1 has no momenta, varying it simply gives the constraint

$$C_1 = V_0 - \frac{b}{\rho} n_i l_b. \tag{14}$$

This is Poisson's equation (averaged) for this variational system. C_1 is the electric field at the cathode and, as we shall shortly see, it vanishes for the two standard equilibria, as expected.

Another constant of motion, when V_0 is time-independent, is the energy function, which is

$$\begin{aligned} H = {} & n_i \left[6\frac{b}{\rho}\left(\dot{b} - \frac{1}{2}\frac{b\dot{\rho}}{\rho} \right)^2 + \frac{1}{2}\frac{b^3}{\rho^3}\dot{\rho}^2 \right] \\ & + \frac{1}{n_i}\left[\frac{\rho}{2b}\left(\frac{\rho}{b}P_{a1} + \frac{1}{2}P_{a2} \right)^2 + \frac{1}{24}\frac{\rho}{b}P_{a2}^2 \right] + bP_{a2} + \rho P_{a1} \\ & - C_1^2 \frac{2b}{l_b}(1 - \tfrac{3}{4}b) + C_1 V_0 \frac{4b}{l_b^2}(1 - \tfrac{3}{4}b) - V_0^2 \frac{6}{l_b^2}(1 - \tfrac{2}{3}b) \\ & - n_i V_0 \frac{2b^2}{\rho l_b} - n_i C_1 \frac{4b^2}{\rho l_b}(1 - \tfrac{3}{4}b) + 2\frac{b^3}{\rho} n_i. \end{aligned} \tag{15}$$

The equations of motion for b and ρ are obtained upon varying b and ρ in (10). These are

$$\begin{aligned} & 12\frac{b}{\rho}\ddot{b} - 6\frac{b^2}{\rho^2}\ddot{\rho} + \frac{6}{\rho}\left(\dot{b} - \frac{b}{\rho}\dot{\rho} \right)^2 - \frac{2}{n_i l_b^3}(1 - b)(V_0 - C_1)^2 \\ & \quad - \frac{4V_0 b}{\rho l_b^2}(1 - \tfrac{1}{4}b) - \frac{8C_1 b}{\rho l_b^2}(1 - b)(1 - \tfrac{3}{8}b) \\ & \quad + 6\frac{b^2}{\rho} - \frac{\rho}{6b^2 n_i^2}\left(P_{a2} + 3\frac{\rho}{b}P_{a1} \right)^2 + \frac{1}{n_i}P_{a2} = 0, \end{aligned} \tag{16}$$

https://doi.org/10.1017/S0022377897005503 Published online by Cambridge University Press

$$4\frac{b^3}{\rho^3}\ddot{\rho} - 6\frac{b^2}{\rho^2}\ddot{b} - 6\frac{b}{\rho^2}\left(\dot{b} - \frac{b}{\rho}\dot{\rho}\right)^2 + 2d\frac{b^2V_0}{\rho^2 l_b}$$
$$+4\frac{b^2C_1}{\rho^2 l_b}(1 - \tfrac{3}{4}b) - 2\frac{b^3}{\rho^2} + \frac{1}{6bn_i^2}\left(P_{a2} + 3\frac{\rho}{b}P_{a1}\right)^2 + \frac{1}{n_i}P_{a1} = 0. \tag{17}$$

These nonlinear equations (16) and (17) describe how the model sheath parameters will evolve, given initial conditions, with C_1 being given by (14). Except for the possible existence of interesting limit cycles, we should expect any evolution of these equations to eventually converge to some equilibrium solution, or a fixed point, where all time derivatives vanish (providing V_0 also becomes a constant value as $t \to \infty$). These may be found by setting $\dot{b} = 0 = \dot{\rho}$ in the above and using (14). The possible equilibrium values for b and ρ can be obtained in the following parametric form:

$$n_i = \rho_0(1 - \tfrac{1}{2}Z_1 + \tfrac{1}{12}Z_2^2), \tag{18}$$

$$V_0 = b_0(1 - \tfrac{1}{2}b_0)\frac{n_i}{\rho_0} - \tfrac{1}{6}b_0 Z_2(1 + \tfrac{1}{3}Z_2), \tag{19}$$

where b_0 and ρ_0 are the equilibrium values of b and ρ, and

$$Z_1 = -2\frac{\rho_0^2}{n_i b_0^3}P_{a1} - \frac{\rho_0}{n_i b_0^2}P_{a2}, \tag{20a}$$

$$Z_2 = 3\frac{\rho_0^2}{n_i b_0^3}P_{a1} + \frac{\rho_0}{n_i b_0^2}P_{a2}. \tag{20b}$$

Owing to the nonlinear structure of (18)–(20), it is not clear that for a given V_0, n_i, P_{a1} and P_{a2}, there will be a unique solution for the equilibrium values of b_0 and ρ_0. However, in the case where $P_{a1} = 0 = P_{a2}$, the equilibrium solution is unique and does reduce to

$$n = n_i/\rho_0 = 1, \tag{21a}$$

$$V_0 = b_0(1 - \tfrac{1}{2}b_0), \tag{21b}$$

which is just the Brillouin case, in our normalized units. In this case, regardless of the initial values of b, ρ and n_i, the system will cause the cathode to either supply or absorb the electrons necessary to achieve the Brillouin density with a sheath thickness compatible with the applied voltage V_0.

This configuration is linearly stable within our model because if we perturb (14), (16) and (17) about this equilibrium point then the eigenfrequencies are given by

$$1 - b_0 - 2\omega^2(1 - \tfrac{1}{2}b_0) + \omega^4 = 0, \tag{22}$$

which has only real roots for the physical range $0 < b_0 < 1$.

Let us now consider the numerical solution of (14), (16) and (17) for an initially empty device with a zero initial voltage and where the conserved momenta (13) are zero. We shall study the evolution of this system as the voltage V_0 is turned on. In this case, initially we have $b = 0$ and $\rho = n_i = 1$. However, (16) and (17) are singular for these initial values, and we cannot turn on the voltage too rapidly without driving the parameters b and ρ into unphysical (negative) values. However, we can easily show that if we turn on the voltage exponentially slowly, then these values remain physical and do behave as we should expect. Let us take the applied

https://doi.org/10.1017/S0022377897005503 Published online by Cambridge University Press

voltage to be of the form

$$V_0(t) = \frac{V_f e^{\gamma t}}{e^{\gamma t} + V_f}, \tag{23}$$

where γ is the inverse of the rise time for the applied voltage and V_f is the final value for the applied voltage. Then, for large negative times, we find that the solutions of (16) and (17) are

$$b(t) = V_0(t) + O(V_0^2), \tag{24a}$$

$$\rho(t) = \frac{n_i}{1 - 3\gamma^2} + O(V_0^2). \tag{24b}$$

We note that in the limit of large negative times, the initial value of ρ is shifted from n_i to a larger value, depending on the rise time of the voltage. However, this solution remains physical providing the rise time is longer than $3^{1/2}$. This restriction is quite reasonable for an actual device, since typical rise times are many cyclotron periods, for which γ would be much less than unity. Thus, for an applied voltage of the form (23), (24) allows us to move off the singular point where V_0 is zero to a final voltage of V_f.

A typical numerical result is shown in Fig. 2 for $\gamma = 0.3$, $n_i = 1.0$ and $V_f = 0.255$. In Fig. 2(a), we see that the sheath thickness rises smoothly from 0 to a final asymptotic value of 0.30, in accordance with (21b). In Fig. 2(b), we see the evolution of the electric field at the cathode. We note that initially it goes slightly positive, which is necessary in order to draw electrons out of the cathode in order to populate the interelectrode space. Then it drops back to essentially zero as the equilibrium is established. In Fig. 2(c) we see that the electron density starts from an initial value of 0.73, consistent with the initial value of ρ in (24b). It then smoothly rises to the Brillouin value of 1.0. The electron drift velocity at the top of the sheath is shown in Fig. 2(d). It rises smoothly also from an initial value of 0 to the Brillouin value of 0.30. Although not shown, the electron drift velocity at the cathode was found to be essentially zero for all time, within the numerical error. Lastly, in Fig. 2(e), we show the evolution of the energy function of the electrons in the vacuum region. We see it smoothly dropping from 0 to a final value of $-0.431\,97$.

Thus the numerical solutions of (16) and (17) verify that these equations do excellently model the evolution of the background density in a crossed-field device. Let us now look at a more general situation.

As mentioned earlier, if before start-up, a device happened to contain some free orbiting electrons then we could expect P_{a1} and P_{a2} to be non-zero initially. Even if these values were small, we should obtain a different equilibrium.

Let us take a case where we have some residual electrons left in a device at zero applied voltage. Let $b = 0.1$, $\rho = 1.0$ and $n_i = 0.2$, which corresponds to a thin, underdense layer of electrons next to the cathode. In this case, we have from (18)–(20) that $P_{a_0} = -0.013\,92$ and $P_{a_2} = -0.000\,87$, giving the initial values of the conserved momenta as non-zero. We now numerically integrate (16) and (17). We use the same model for the applied voltage (23) as before. But, since this initial condition is not a singular point, we do not need to use (24), and shall use instead the above initial values. The results are shown in Fig. 3, and are strikingly different from the results in Fig. 2.

In Fig. 3(a), we see the evolution of the sheath thickness from 0.1 to its final form. What is clearly evident here is the existence of a stable limit cycle. In Fig. 3(b),

https://doi.org/10.1017/S0022377897005503 Published online by Cambridge University Press

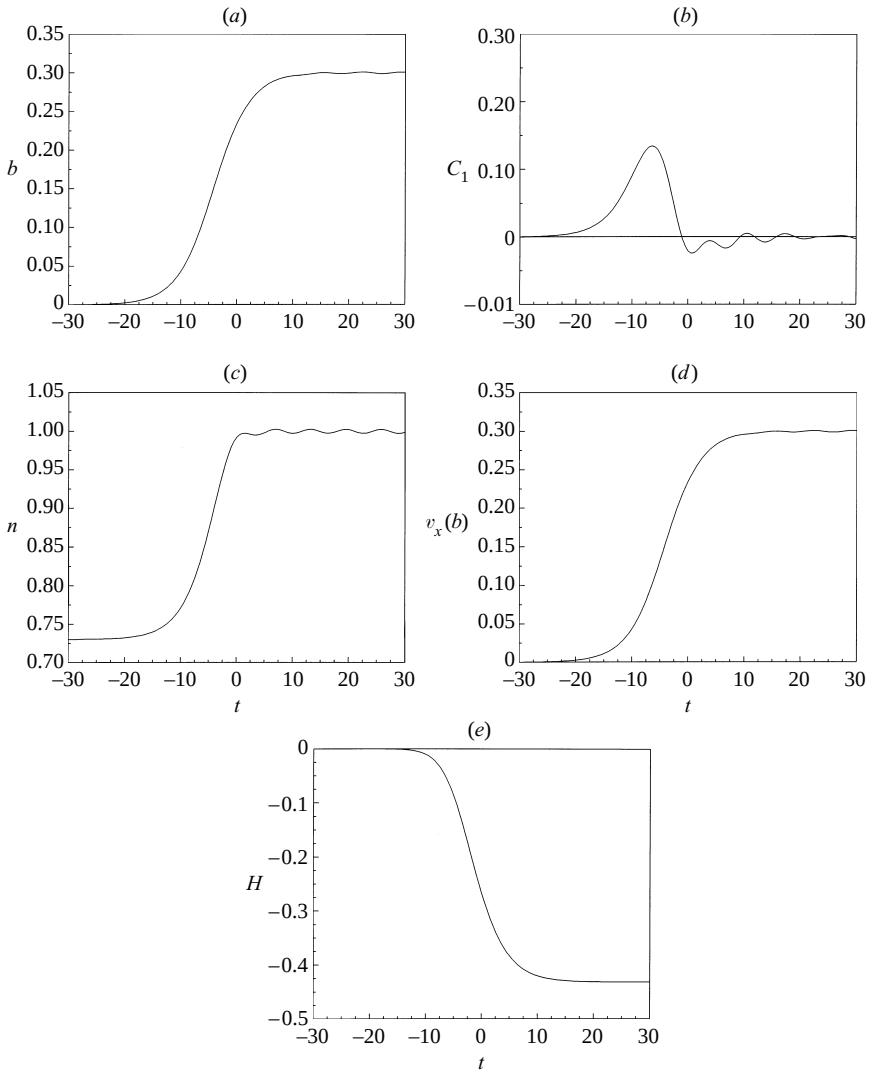


Figure 2. The numerical solution of (14), (16) and (17) using the applied voltage (23) and the resulting initial values given by (24). The parameters used were $\gamma = 0.3$, $n_i = 1.0$ and $V_f = 0.255$. In this figure, b the sheath thickness, C_1 is the electric field at the cathode, n is the sheath density, $v_0(b)$ is the drift velocity at the top of the sheath and H is the energy function. Not shown is the electron drift velocity at the cathode, which was zero for all time within the numerical error of 10^-7.

we see the evolution of the electric field at the cathode. We observe that it is initially negative, consistent with (14) for a zero initial voltage. We can understand this physically by noting that if there were electrons present initially then they would set up an opposing electric field, which would prevent other electrons from emerging from the cathode. Furthermore, owing to their self-electric field, they would drift in the negative x direction. In a planar device, this will be a stable configuration, because the linear momentum is conserved and is negative. The electrons simply cannot decay to the cathode without somehow losing their linear

https://doi.org/10.1017/S0022377897005503 Published online by Cambridge University Press

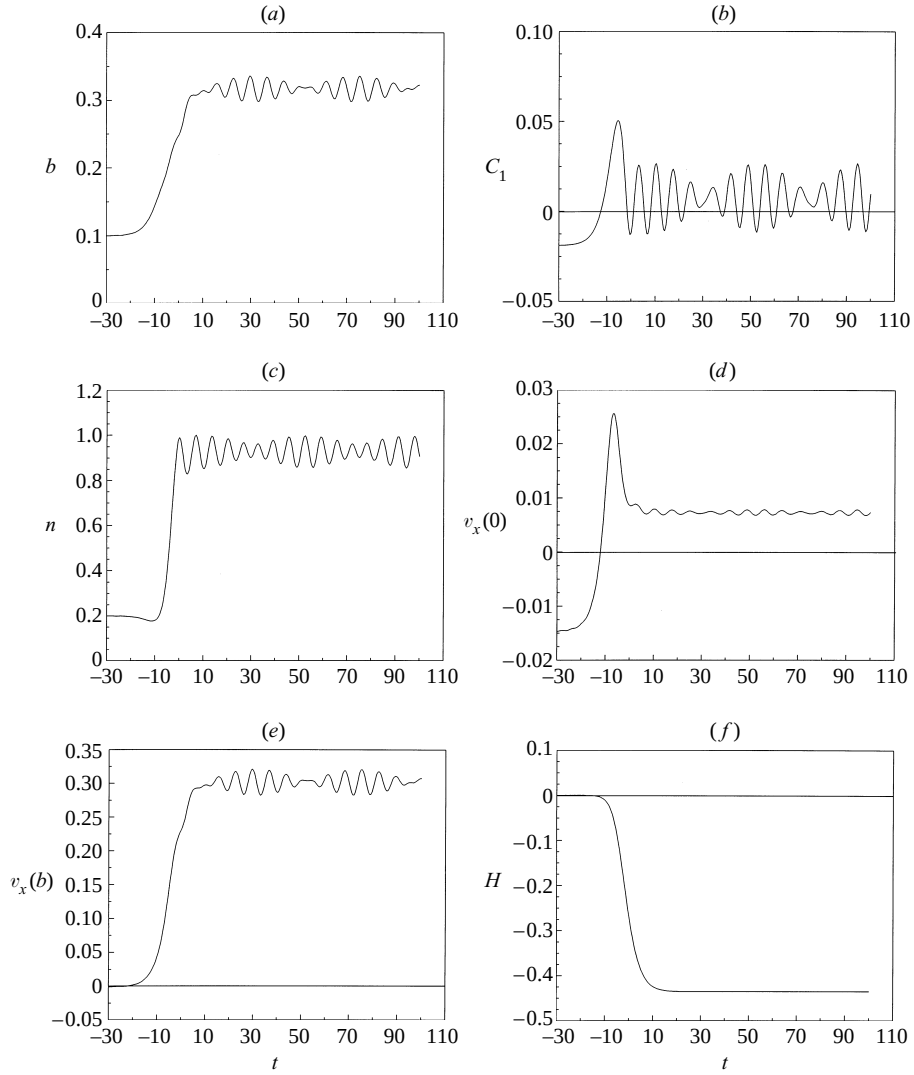


Figure 3. The numerical solution of (14), (16) anbd (17) for the initial values of $b = 0.1$, $n_i = 0.2$ and $\rho = 1.0$ using the applied voltage (23), with the parameters $\gamma = 0.3$ and $V_f = 0.255$ as in Fig. 2. The plots are of the same quantity as in Fig. 2, except that we also show the electron drift velocity at the cathode, $v_0(0)$.

momentum. Similarly, for a cylindrical device, this would be a stable configuration owing to conservation of the electrons angular momentum. In Fig. 3(*c*), we see the evolution of the density. It starts from 0.2 and evolves toward the stable limit cycle, where the density remains *below* the Brillouin value of 1.0. In Fig. 3(*d*), we show the evolution of the electron drift velocity at the cathode. As remarked above, it is initially negative and approaches the limit cycle, where it has a very small positive value of about 0.007. In Fig. 3(*e*), we see the electron drift velocity at the top of the sheath. It rises from a very small negative value to the limit cycle, where it oscillates about 0.30. What we should observe here is that, because of the limit cycle, the electrons at the top of the sheath can never remain in phase with the phase

https://doi.org/10.1017/S0022377897005503 Published online by Cambridge University Press

velocity of any RF electric field on the anode. Rather, at best, they would move in and out of resonance owing to the limit cycle. Thus we need not expect any such RF wave to be amplified when any such a limit cycle is present. In Fig. 3(f), we see the evolution of the energy function H. It starts from an initial value of $-0.000\,08$ and evolves to the asymptotic value of $-0.435\,82$, which lies *below* the above value for Brillouin flow of $-0.431\,97$. Thus this state with a limit cycle has a slightly lower energy that the Brillouin state. However, this lower-energy state with its limit cycle can only be reached if the conserved linear momentum is non-zero.

Now it needs to be mentioned that limit cycles may well not be stable in an actual device. Our current variational model is limited, since it has only a limited number of degrees of freedom. The addition of more degrees of freedom may well allow mixing to occur, in which case we should expect the limit cycles to decay. However, at present this is not known, and furthermore there is the problem that the above limit-cycle flow does have a lower energy than the Brillouin flow. So, if it did decay, it could not decay into the Brillouin flow without somehow picking up a small amount of energy from somewhere. Thus it could well be that, under certain initial conditions as above, limit cycles could appear and could be a source of a disturbance in the normal operation of a device.

4. RF modes

Let us now assume that we have a classical background equilibrium where $P_{a_1} = P_{a_2} = 0$ (and thus $Z_1 = 0 = Z_2$) and

$$V_0 = b_0(1 - \tfrac{1}{2}b_0), \tag{25a}$$

$$n = 1, \tag{25b}$$

$$C_1 = 0. \tag{25c}$$

Under these conditions, we can evaluate the model Lagrangian (9) for an RF wave present where e_1, f_1, μ and ν are non-zero. This will give us four nonlinear equations of motion for e_1, f_1, μ and ν. Because their complexity, we shall not present these equations here, but their derivation is described in Appendix A. However, the most important aspect of these equations is their small-amplitude solutions, because these would govern the initial evolution of an RF plasma wave being driven by an RF wave in the slow-wave structure. The linearized forms of these equations have constant coefficients, whence we may analyse them using Fourier analysis. The resulting four equations reduce to

$$C_{ee}e_1 + C_{ef}f_1\cos\delta + C_{ev}V_1\cos\mu = 0, \tag{26a}$$

$$C_{ff}f_1 + C_{ef}e_1\cos\delta + C_{fv}V_1\cos\nu = 0, \tag{26b}$$

$$e_1(C_{ef}f_1\sin\delta - C_{ev}V_1\sin\mu) = 0, \tag{27a}$$

$$f_1(C_{ef}e_1\sin\delta + C_{fv}V_1\sin\nu) = 0, \tag{27b}$$

where $\delta = \nu - \mu$ and

$$C_{ee} = -2l_b\omega^2 + 3bl_b\omega k - \tfrac{6}{5}b^2l_bk^2, \tag{28a}$$

$$C_{ef} = 2l_b\omega - \tfrac{3}{4}bk, \tag{28b}$$

$$C_{ff} = -2l_b\omega^2 + 3bl_bwk - \tfrac{3}{2}b^2l_bk^2 - \frac{3b}{2l_b}(1 - \tfrac{2}{3}b), \tag{29}$$

https://doi.org/10.1017/S0022377897005503 Published online by Cambridge University Press

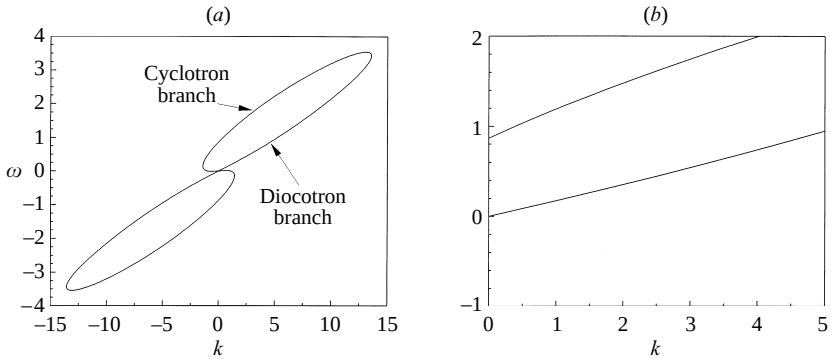


Figure 4. The dispersion curves of ω versus k for the RF modes when $b = 0.3$: (a) global solution; (b) solution in the physical regime.

$$C_{ev} = \tfrac{3}{4} b l_b k^2, \tag{30}$$

$$C_{fv} = -\tfrac{3}{10} v^2 l_b k^2 + 3(1 - \tfrac{2}{3} b), \tag{31}$$

and V_1 is the relative RF voltage at the anode. When V_1 is zero, there is only one possible solution, and that is for

$$\mu = \nu, \tag{32a}$$

$$C_{ee} e_1 + C_{ef} f_1 = 0, \tag{32b}$$

$$C_{ee} C_{ff} - C_{ef}^2 = 0. \tag{32c}$$

Equation (32c) is the dispersion relation for this mode. It is a quartic in both ω and k, and is

$$\begin{aligned} &4 l_b^2 \omega^4 - 12 b l_b^2 \omega^3 k + \tfrac{72}{5} b^2 l_b^2 \omega^2 k^2 \\ &- \tfrac{81}{10} b^3 l_b^2 \omega k^3 + \tfrac{9}{5} b^4 l_b^2 k^4 - 4(1 - \tfrac{3}{4} b)\omega^2 \\ &+ 3b(1-b)^2 \omega k - \tfrac{9}{16} b^2 (1 - \tfrac{16}{5} b^2 + \tfrac{32}{15} b^2) k^2 = 0. \end{aligned} \tag{33}$$

Plots of the frequency versus k for this mode are shown in Figs 4(a, b) for $b = 0.3$. Figure 4(a) gives the global solution, while Fig. 4(b) gives the solution in the parameter regime of interest. The ratio of the y and x amplitudes f_1/e_1 is shown in Fig. 5.

Consider Fig. 4(b). There are two branches of this dispersion curve. First, the long straight middle segment, which has a slope of approximately $\frac{1}{2} b$, corresponds to the diocotron mode where $\approx \frac{1}{2} v_0 k$, with v_0 the drift velocity of the top of the sheath. The electron motion along this segment is essentially a longitudinal oscillation parallel to the cathode, with a smaller component transverse to the cathode, as can be seen from Fig. 5. Thus the net motion is that of a flattened ellipse. Above this branch is another branch of a cyclotron-like mode, where $\omega \approx \pm\Omega + \frac{1}{2} k v_0$. This mode has roughly equal x and y amplitudes, giving a net electron motion that is essentially circular.

Considering the above comments, one sees that there is a defect in this variational model in that the slopes of both branches are roughly one-half of what they should be. The reason for this is found in the choice of trial functions. Since we choose the amplitudes of the electron RF oscillations to be proportional to y (see (2)), the RF wave is forced to sample motion throughout the entire sheath, not simply on the

https://doi.org/10.1017/S0022377897005503 Published online by Cambridge University Press

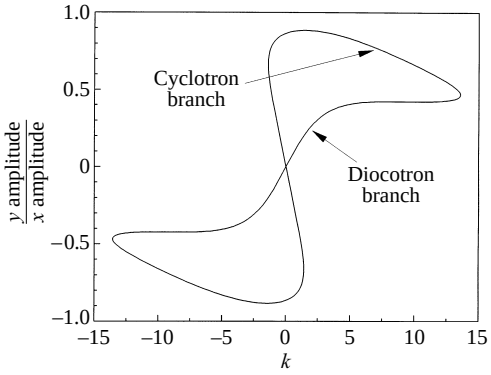


Figure 5. The ratio of the y to x amplitudes versus k for the RF modes shown in Fig. 4. The phase is such that when the ratio is positive, the particle rotates clockwise.

top layer. Consequently, the phase velocity of this wave is an average over all drift velocities in the sheath, not just the top layer, whence the factor of roughly $\frac{1}{2}$ and not unity.

Although this defect will affect numerical and quantitative values, the qualitative behaviour is quite strikingly similar to what we should expect. It is interesting to compare this variational solution with that obtained from the cold-fluid equations with a Brillouin flow. As long as we keep ω and k small and in the operating range of a typical device, we can WKB (Wentzel–Kramers–Brillouin) the cold-fluid equations and obtain its dispersion relation. The WKB solution is derived in Appendix B for this situation, and the resulting dispersion relation for $b = 0.3$ is represented by the two outer (solid) curves in Fig. 6. We can observe that the upper branch is the analogue of the cyclotron branch of Fig. 4(*b*). What is missing from Fig. 4(*b*) is the lower cyclotron branch shown in Fig. 6. The easiest way to explain the missing branch is simply to say that the trial orbitals chosen cannot adequately model the electron motion along this branch, while, at the same time, they can apparently model the motion along the upper branch. This is not at all unreasonable, since the electrons along these two branches execute circular motion, but in opposite directions (see Appendix B). Our trial orbitals are basically laminar, but, owing to the background shear flow, such orbitals can apparently adequately approximate a clockwise circular motion (which the upper branch executes) but not a counter-clockwise circular motion (which the lower branch executes). However, as we have already remarked, both these cyclotron modes are *outside* the physical parameter regime. Thus there is no real need to attempt to model them.

Now, let us address the diocotron branch. In the cold-fluid equations with a pure Brillouin flow, this branch is absent. Such a model has *only* the two cyclotron branches, shown in Fig. 6. The dashed line shown in Fig. 6 had to be calculated for a *non*-Brillouin flow, the 'double-box' model, introduced by us (Kaup and Thomas 1992*b*). A comparison of these two density profiles is shown in Figs 7 and 8. Figure 7 shows the Brillouin density profile, while Fig. 8 shows the double-box density profile. Note that they only differ at the edge. The double-box parameters used to calculate the dashed curve in Fig. 6 were a Brillouin flow for the lower box, with a thickness of $b = 0.295$. The parameters for the second box were a density of $n_2 = 0.5$, with a thickness of $\delta = 0.01$. (This double-box model also has essentially the same two cyclotron branches as the pure Brillouin flow.) Of course, the difference between

https://doi.org/10.1017/S0022377897005503 Published online by Cambridge University Press

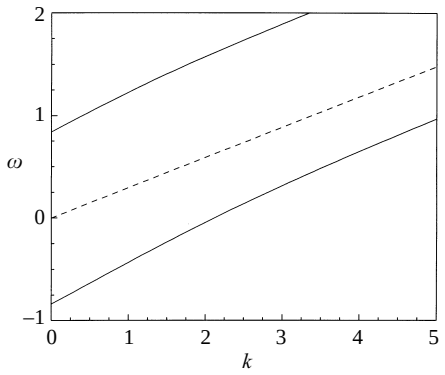


Figure 6. The dispersion curves for a pure Brillouin flow (solid lines) and the diocotron mode of a double-box profile (dashed line). The sheath thickness is $b = 0.3$ for the Brillouin flow. For the double-box profile, we have used a Brillouin flow for the inner box, with $b = 0.295$, and for the second box, a thickness (δ) of 0.01 with a density of 0.05. The double-box profile also has the same cyclotron modes as the pure Brillouin flow.

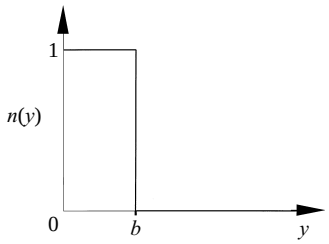


Figure 7. The density profile for a Brillouin flow. It is of a box shape where the width is b and the height is unity in our normalized units.

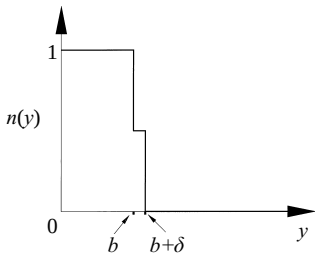


Figure 8. The double-box density profile for small δ, where δ is the width of the second box. The density of the second box is $\frac{1}{2}$.

the pure Brillouin profile and the double-box profile used here is very slight – they only differ at the edge of the sheath. However, this slight difference has a profound effect on the existence of the RF modes. For the Brillouin profile, there is no diocotron mode. For the double-box profile, there is a diocotron mode, even when δ is vanishingly small, but non-zero. Obviously, one concludes from this that small changes in the structure of the edge of the sheath can have profound effects on the modal structure. The only models that predict a diocotron branch are the double-box model and the present variational model.

https://doi.org/10.1017/S0022377897005503 Published online by Cambridge University Press

5. Concluding remarks

We have presented a Raleigh–Ritz variational method for modelling crossed-field devices. In many ways, this model closely models the cold-fluid equations. However, there are several significant ways in which they differ. First, it should be noted that this variational principle is based on a very simplified Vlasov model, in that we vary electron orbits. In the case of the background solution, variations of the electron orbits include an extremization against vertical motions, which is analogous to first-order vertical perturbations of the cold-fluid equations. Thus it is then not at all surprising that the variational model, at lowest order, contains some results from the higher-order cold-fluid equations, such as an equilibrium density equal to the Brillouin limit, thereby giving a unique profile.

The diocotron mode does not occur in the cold-fluid theory with a pure Brillouin density profile, although analogies of the cyclotron modes are known. However it is known that if one simply very slightly modifies the pure box profile into a 'double-box' profile, then the diocotron mode suddenly appears in the cold-fluid theory (Kaup and Thomas 1992*b*). The reason for this is that the diocotron mode requires at least a very thin layer of electrons with a different density on top of the sheath before it can appear. For a pure box density profile with an infinite density gradient at the edge of the sheath, this is not possible. But, for the double-box profile, there is a step in the density profile at the edge of the sheath, which then allows the diocotron mode to exist – and it exists even when the width of the step is vanishing small but non-zero.

This same effect is present in this variational model. Consider the electron orbits in (2) with an RF wave present. All electrons have an oscillating up-and-down motion. Near the edge, there will be locations in space through which some but not all the electron orbits pass. Thus, although our *initial* distribution was a pure box (see (17)), the succeeding RF oscillations introduce a structure on the edge of the density profile, which would average to a lower density, necessary for the existence of the diocotron mode.

We have also demonstrated that the variational principle provides a means of studying the interactions inside crossed-field devices. The simple model of electron orbits given in (2) allows one to obtain physically reasonable background solutions and also reasonable dispersion curves for the RF modes. Clearly, there are improvements that could be made in the model – in particular, the quantitative prediction of the group velocities of the RF waves. However, comparison of Figs 4(*b*) and 6 reveals that for the physical mode (diocotron) of interest, the qualitative agreement is excellent. And, at the same time, there are mathematical advantages to be gained in keeping a model as simple as possible.

Acknowledgements

This research was supported in part by the Air Force office of Scientific Research under Grant F49620-93-1-0088 and by the Naval Surface Warfare Center, Crane Division. The analytical computations were performed with the assistance of MACSYMA, a symbolic computational software (obtainable from Macsyma, Inc., 20 Academic Street, Arlington, MA 02174, USA).

https://doi.org/10.1017/S0022377897005503 Published online by Cambridge University Press

Appendix A

We shall now describe the key details required for evaluating the Lagrangian (9). First, we treat the background case where the RF field is absent. Differentiating (2) and using (6), upon eliminating the Lagrangian displacements, we have the velocities given by

$$v_{xj} = \dot{a}_0 + \dot{a}_1 \left(\xi_b - \frac{b - y_j}{\rho} \right), \tag{A 1a}$$

$$v_{yj} = \dot{b} - \frac{\dot{\rho}}{\rho}(b - y_j). \tag{A 1b}$$

From (4), upon matching the electrostatic potential and its derivative at the edge of the sheath, we have

$$\phi_l = C_1 y + \frac{y^2}{b(2l - b)}(V_0 - \tfrac{1}{2} l C_1) \quad (0 < y < b), \tag{A 2a}$$

$$\phi_u = V_0 - (l - y)\frac{2V_0 - bC_1}{2l - b} \quad (b < y < l). \tag{A 2b}$$

The last term in (9) is now easily found, using the appropriate form from (A 2), integrating y from 0 to b, and then from b to l. For the particle part, we transform variables from the Lagrangian displacements to the particle coordinates, noting that the Jacobian of the transformation is simply $1/\rho$. Then we integrate y_j from 0 to b, and, upon rescaling as described after (9), we obtain (10).

Obtaining (26) and (27) is a bit more complex. As above, we first obtain the particle velocities as functions of the variational parameters. For this calculation, we take the background to be static. Then, from (2), (3) and (6), we find

$$\begin{aligned} v_{xj} = \frac{y_j}{D}\{&(1 + f_1 \cos\theta_y)[\dot{e}_1 \sin\theta_x - e_1(\dot{\mu} + \omega)\cos\theta_x] \\ &- e_1 \sin\theta_x [\dot{f}_1 \cos\theta_y + f_1(\dot{\nu} + \omega)\sin\theta_y]\} \end{aligned} \tag{A 3a}$$

$$\begin{aligned} v_{yj} = {} & \frac{-y_j}{1 + f_1 \cos\theta_y}[\dot{f}_1 \cos\theta_y + (\dot{\nu} + \omega) f_1 \sin\theta_y] \left(1 + \frac{k y_j f_1 e_1}{D} \sin\theta_x \sin\theta_y \right) \\ & + \frac{k y_j^2 f_1}{D} \sin\theta_y [\dot{e}_1 \sin\theta_x - e_1(\dot{\mu} + \omega)\cos\theta_x], \end{aligned} \tag{A 3b}$$

where

$$D = 1 + f_1 \cos\theta_y - e_1 k y_j [\cos\theta_x + f_1 \cos(\mu - \nu)]. \tag{A 4}$$

For matching the electrostatic potential and its derivative at the top of the sheath, we need the position of the surface of the sheath as a function of x. This follows from (2), where we have

$$y_{jb} \equiv y_j(\xi_y = \xi_b) = \frac{b}{1 + f_1 \cos\theta_y}, \tag{A 5}$$

where the x dependence follows from (3b). Then we obtain

$$C_2 = \frac{V_0(1 + V_1 \cos\theta) - l C_1}{y_{jb}(2l - y_{jb})}, \tag{A 6a}$$

$$d_1 = \frac{2V_0(1 + V_1 \cos\theta) - C_1 y_{jb}}{2l - y_{jb}} \tag{A 6b}$$

for the two coefficients C_2 and d_1, which, with (4), gives the required solution for

https://doi.org/10.1017/S0022377897005503 Published online by Cambridge University Press

the electrostatic potential. As before, the last term in (9) is now easily found, using the appropriate form from (4), except that we now integrate y from 0 to y_{jb}, and then from y_{jb} to l. There still remains an x integration to be done, which we shall discuss shortly.

For the particle part, we transform again variables from the Lagrangian displacements to the particle coordinates. In this case, the Jacobian of the transformation is D/ρ and the integration is only from $y_j = 0$ to y_{jb}.

Once these y integrations have been done, we are still left with an overall x integration. The x dependence enters parametrically through the θs, and consequently is periodic. So we can simply integrate over one period, or, equivalently, average the result of the y integrations. When we study the structure of the required integrals, although they can in principle be found, the resulting expressions are too complex to be of any value except for numerical computations. However, we can expand in powers of the RF amplitudes, e_1 and f_1, expanding them to second order. Then it becomes a trivial matter to average the trigonometric functions. From these, we can then obtain (26) and (27). The calculus and algebra required for obtaining (26) and (27) is quite long and tedious; however, we have found that it is very easy to do with the aid of MACSYMA.

Appendix B

It is straightforward to obtain a WKB solution for the cold-fluid equations when ω and k are in the physical operating regime of a crossed-field device. We start with the equations given in Kaup and Thomas (1989) for the first-order fundamental mode. These are

$$\partial_y p = Au, \tag{B 1a}$$

$$\partial_y u = Bp, \tag{B 1b}$$

where

$$A = \Omega^2 - \omega_e^2, \tag{B 2}$$

$$B = \frac{k^2}{A} - \frac{k\partial_y n_0}{\Omega\omega_e A} - \frac{2k^2 n_0 \Delta^2}{\Omega^2 A^2}, \tag{B 3}$$

$$\omega_e = \omega - kv_0, \tag{B 4}$$

$$v_0 = \partial_y \phi_0 / \Omega, \tag{B 5}$$

$$\partial_y^2 \phi_0 = n_0, \quad \phi_0(0) = 0 = \partial_y \phi_0(0), \tag{B 6}$$

$$\Delta^2 = \Omega^2 - n_0, \tag{B 7}$$

$$u = -ikv_{1x}, \tag{B 8}$$

$$p = Av_{1y}. \tag{B 9}$$

In the above, the subscript '0' indicates a background quantity and (B 4)–(B 7) are the definitions for a general (non-Brillouin) density profile n_0. ω_e is the frequency of the RF wave as seen by the moving electron. Δ is the local oscillating frequency for individual electrons (Prasad *et al.* 1987; Kaup and Thomas 1992*a*), which vanishes for a Brillouin flow. In (B 8) and (B 9), v_{1x} and v_{1y} are the x and y components of the perturbed velocity fields. The perturbed electrostatic potential ϕ_1 and the

https://doi.org/10.1017/S0022377897005503 Published online by Cambridge University Press

perturbed electron density n_1 are obtained from p and u as follows:

$$n_1 = ip\left(\frac{2kn_0^2}{\Omega A^2} - \frac{\partial_y n_0}{A\omega_e}\right), \tag{B 10}$$

$$\phi_1 = \frac{ip\Delta^2}{Ak\Omega} - \frac{iu\omega_e}{k^2}, \tag{B 11}$$

$$\partial_y\phi_1 = \frac{i\Omega}{k}u - \frac{i\omega_e}{A}p. \tag{B 12}$$

The boundary conditions on (B 1) follow from the boundary conditions on ϕ_1. At the cathode, which is grounded, the perturbed potential must vanish. Thus $\phi_1(y = 0) = 0$. At the anode, we shall use the 'smooth-bore' approximation, in which we take $\phi_1(y = l) = 0$.

For the Brillouin case, we have two regions – one inside the sheath and other outside it (see Fig. 7). Outside the sheath, the solution is simply the vacuum solution. Inside the sheath, the coefficient A can vary as a function of y. Thus it is possible for A to have a simple zero inside the sheath, which then would give a regular singular point to (B 1*b*). This singular point was thoroughly studied in Buneman *et al.* (1966). However, it will be important only for high k, which is well outside the standard operating range of such devices. Note that, for standard devices, ω is usually less than Ω. Also, at the cathode, ω_e initially decreases as y increases when $\omega > 0$. Thus A cannot have a zero until kv_0 becomes at least as large as Ω. But this would then be outside the known operating parameter region. Thus, as long as we limit our attention to the design operating range, we can ignore the possibility of zeros for A.

The WKB solution of (B 1) inside a Brillouin sheath is therefore

$$p = C_4\, A^{1/2}\, \cosh(ky), \tag{B 13a}$$

$$u = \frac{kC_4}{A^{1/2}}\, \sinh(ky), \tag{B 13b}$$

where C_4 is an arbitrary constant. In matching across the density discontinuity to the vacuum region above the sheath, we integrate (B 1) and find that p is continuous while u has a discontinuity. Thus, just above the sheath, our solution becomes

$$(b + 0) = C_4\, A_f^{1/2} \cosh(kb), \tag{B 14a}$$

$$u(b + 0) = \frac{kC_4}{A_f^{1/2}}\left[\sinh(kb) + \frac{\Omega}{\omega_{ef}}\cosh(kb)\right], \tag{B 14b}$$

where $A_f = A(y = b)$ is the value of A at the top of the sheath, and $\omega_{ef} = \omega_e(y = b)$ is the value of ω_e at $y = b$. It should be noted here that the integration across the discontinuity is perfectly valid provided that ω_e and A do not vanish at or near the discontinuity.

From (B 11) and (B 12), we can construct the electrostatic potential in the vacuum region above the sheath. This gives

$$\phi_1 = \frac{iC_4\Omega}{k\, A_f^{1/2}}\left\{\left[\sinh(kb) + \frac{A_f}{\Omega\omega_{ef}}\cosh(kb)\right]\sinh[k(y - b)] - \frac{\omega_{ef}}{\Omega}\sinh(kb)\cosh[k(y - b)]\right\}. \tag{B 15}$$

https://doi.org/10.1017/S0022377897005503 Published online by Cambridge University Press

Using the smooth-bore boundary condition at the anode, ϕ_1 has to vanish at $y = l$. This gives an equation quadratic in ω_{ef}, namely

$$(\Omega^2 - \omega_{ef}^2)\tanh[k(l-b)] - \omega_{ef}^2 \tanh(kb) + \Omega\omega_{ef}\tanh[k(l-b)]\tanh(kb) = 0 \quad \text{(B 16)}$$

It is a simple matter to solve (B 16) for ω as a function of k. A plot of ω versus k using scaled variables is shown in Fig. 6 for $b = 0.3l$, a typical value.

To determine the sense of particle rotation along either branch, we need the Lagrangian displacements of the fluid particles (Drazin and Reid 1981). These are related to the velocities by

$$\Xi_y = iv_{1y}/\omega_e, \quad \text{(B 17}a\text{)}$$

$$\Xi_x = i(\Xi_y\Omega + v_{1x})/\omega_e. \quad \text{(B 17}b\text{)}$$

Evaluating the ratio of these two quantities along the two branches above gives the rotation sense discussed in the main text.

References

Antonsen, T. M., Ott, E., Chang, C. L. and Drobot, A. T. 1985 *Phys. Fluids* **28**, 2878.

Bogema, B. L. and Davidson, R. C. 1970 *Phys. Fluids* **13**, 2772.

Brillouin, L. 1945 *Phys. Rev.* **67**, 260.

Buneman, O. 1955 *J. Electronics* **1**, 314.

Buneman, O., Levy, R. H. and Linson, L. M. 1996 *J. Appl. Phys.* **37**, 3203.

Chernin, D. and Lau, Y. Y. 1984 *Phys. Fluids* **27**, 2319.

Christenson, P. J. and Lau, Y. Y. 1994 *Phys. Plasmas* **1**, 3725.

Davidson, R. C. 1985 *Phys. Fluids* **28**, 377.

Davidson, R. C. 1985 *Phys. Fluids* **28**, 1937.

Davidson, R. C. and Krall, N. A. 1970 *Phys. Fluids* **13**, 1543.

Davidson, R. C. and Tang, K. T. 1985 *Phys. Fluids* **28**, 1169.

Dombrowski, G. E. 1988 *IEEE Trans. Electron Devices* **35**, 2060.

Drazin, P. G. and Reid, W. H. 1981 *Hydrodynamic Stability*, pp. 75–76. Cambridge University Press.

Jablonski, M. K. 1992 MSc thesis, MIT.

Kaup, D. J. 1990 *Phys. Fluids* **B2**, 2253.

Kaup, D. J. and Thomas, G. E. 1989 *Stud. Appl. Maths* **81** [*Erratum* **83**, 271(E) (1990)].

Kaup, D. J. and Thomas, G. E. 1992*a* *Phys. Fluids* **B4**, 2640.

Kaup, D. J. and Thomas, G. E. 1992*b* *J. Appl. Phys.* **71**, 5752.

Lau, Y. Y. and Chernin, D. 1992 *Phys. Fluids* **B4**, 3473.

Lau, Y. Y. Christenson, P. J. and Chernin, D. 1993 *Phys. Fluids* **B5**, 4486.

Loveland, R. V. and Ott, E. 1974 *Phys. Fluids* **17**, 1263.

Macfarlane, G. G. and Hay, H. G. 1950 *Proc. Phys. Soc.* **63**, 409.

Palevski, A., Bekefi, G. and Drobot, A. 1981 *J. Appl. Phys.* **52**, 4938.

Prasad, S. A., Morales, G. J. and Fried, B. D. 1987 *Phys. Fluids* **30**, 3093.

Riyopoulos, S. A. 1991 *Phys. Fluids* **B3**, 3505.

Riyopoulos, S. 1993 *Phys. Rev.* **E47**, 2839.

Riyopoulos, S. 1993 *Phys. Fluids* **B5**, 4162.

Riyopoulos, S. A., Chernin, D. P. and Drobot, A. T. 1992 *IEEE Trans. Electron Devices* **39**, 1529.

Swegle, J. 1983. *Phys. Fluids* **26**, 1670.

Swegle, J. and Ott, E. *Phys. Fluids* **24**, 1821.

Thomas, G. E., Bollen, W. M., Kaup, D. J., Goplen B. and Ludeking, L. 1985 *Technical Digest, International Conference on Electron Devices, Washington, DC, 1985*, pp. 180–183. IEEE, New York.

Uhm, H. S. 1992 *Phys. Fluids* **B4**, 740.

https://doi.org/10.1017/S0022377897005503 Published online by Cambridge University Press